

Review

Iron Oxide Labeling and Tracking of Extracellular Vesicles

Yuko Tada  and Phillip C. Yang *

School of Medicine, Department of Medicine, Division of Cardiovascular Medicine and Cardiovascular Institute, Stanford University, 269 Campus Drive, CCSR 3115C, Stanford, CA 94305, USA; ytada@stanford.edu

* Correspondence: phillip@stanford.edu, Tel.: +1-650-498-8008

Received: 30 September 2019; Accepted: 5 November 2019; Published: 7 November 2019



Abstract: Extracellular vesicles (EVs) are essential tools for conveying biological information and modulating functions of recipient cells. Implantation of isolated or modulated EVs can be innovative therapeutics for various diseases. Furthermore, EVs could be a biocompatible drug delivery vehicle to carry both endogenous and exogenous biologics. Tracking EVs should play essential roles in understanding the functions of EVs and advancing EV therapeutics. EVs have the characteristic structures consisting of the lipid bilayer and specific membrane proteins, through which they can be labeled efficiently. EVs can be labeled either directly using probes or indirectly by transfection of reporter genes. Optical imaging (fluorescent imaging and bioluminescent imaging), single-photon emission computed tomography (SPECT)/positron emission tomography (PET), and magnetic resonance imaging (MRI) are currently used for imaging EVs. Labeling EVs with superparamagnetic iron oxide (SPIO) nanoparticles for MRI tracking is a promising method that can be translated into clinic. SPIO can be internalized by most of the cell types and then released as SPIO containing EVs, which can be visualized on T2*-weighted imaging. However, this method has limitations in real-time imaging because of the life cycle of SPIO after EV degradation. Further studies will be needed to validate SPIO labeling by other imaging modalities in preclinical studies. The emerging technologies of labeling and imaging EVs with SPIO in comparison with other imaging modalities are reviewed in this paper.

Keywords: extracellular vesicles; superparamagnetic iron oxide nanoparticles; magnetic resonance imaging (MRI)

1. Introduction

Extracellular vesicles (EVs), which represent microvesicle and exosome secretomes, are produced by most of the cell types under physiological and pathological conditions, playing essential roles in intercellular communications. EVs secreted from cells migrate through interstitial fluid or systemic circulation and transfer their cargos consisting of nucleic acids, proteins, lipids, and mitochondrial fractions to their recipient cells [1–3]. mRNAs from EVs can be translated in the recipient cells and miRNA from EVs can modulate gene expression and biological functions [4]. For instance, cardiomyocytes exchange EVs with cardiac fibroblasts and endothelial cells inside the interstitium. Myocardial function is modified by those interstitial cell-derived EVs in adaptive responses both in beneficial or harmful ways. miR-21* (the passenger strand miRNA), transferred from fibroblast-derived EVs stimulates myocardial hypertrophy [5]. Endothelial cell-derived exosomes increase miR-146a expression level in cardiomyocytes, leading to impaired metabolic activity and contractile dysfunction [6]. EV therapy could modulate and enhance the innate repair capacities. The usefulness of EVs in tissue repair or regeneration have been suggested by many researchers. EVs from bone marrow stem cells modified

the functions of endothelial cells and cardiomyocytes to improve cardiac function with enhanced angiogenesis [7]. Mesenchymal stem cell (MSC)-derived EVs reduced myocardial infarct size following the ischemia reperfusion in animal models [8,9].

Due to their unique characteristics including nano-scale size, biogenesis potential, endogenous lipid bilayer membrane, signal transduction system, and effectors of various biological information, EVs can be useful in numerous ways in diagnostic and therapeutic roles. Furthermore, EV therapy could have distinctive advantages compared to stem cell therapy. They are potentially less toxic and less likely to suffer immune rejections. The dose could be optimized to achieve higher concentration of effectors. Finally, EVs have wider delivery options since EVs have intrinsic capacities to cross tissue and cellular barriers. With higher biocompatibility and less toxicity, EVs may replace artificial lipid nanoparticles in the future as drug delivery vehicles to deliver exogenous and endogenous therapeutic cargos. Due to these potentials of EVs, monitoring the distribution and fate of secreted or implanted EVs in vitro or in vivo is one of the essential strategies in understanding their functions and advancing the EV-mediated diagnostics or therapeutics. Appropriate biodistribution of EVs is key to their efficacy and safety.

Among the existing labeling and tracking technologies including optical imaging, nuclear imaging and magnetic resonance imaging (MRI), labeling with superparamagnetic iron oxide (SPIO) nanoparticles for MRI tracking is a promising method. SPIO are the magnetic nanoparticles, which are clinically used as MRI contrast agents to detect cancers, inflammation, vascular flows, or tissue perfusion [10–12]. In regenerative medicine, stem cells have been successfully labeled with SPIO and tracked after implantation [13–15]. Finally, the technology of labeling and tracking EVs with SPIO is currently under development.

Here, we review the emerging technologies of labeling and imaging EV with SPIO and compare them with other imaging modalities.

2. Extracellular Vesicles

2.1. Microvesicles and Exosomes

Exosomes and microvesicles are two of the major components of EVs, which differ in their size, biogenesis potential, and secretion pathways [16,17]. Exosomes are smaller vesicles (40–150 nm) and technically indicate the vesicles passing through 220-nm pore filters or recovered by high-speed ultracentrifugation. Exosomes are formed in the multivesicular bodies (MVB) and released by the fusion of plasma membrane. In the beginning of this process, cells generate early endosomes by endocytosis. During the maturation to late endosomes, some endosomes shed intraluminal vesicles (ILV) within themselves to become MVBs. MVBs migrate to the cell membrane and fuse with the membrane and release exosomes [18]. By contrast, microvesicles are bigger vesicles compared to exosomes (150–1000 nm) and released from the plasma membrane by budding. However, it is difficult to separate them completely. EVs are released both under physiological and pathological conditions. For instance, adult cardiomyocytes are known to release various sized EVs [19]. Nano-scale EVs can be visualized by electron microscopy (Figure 1). Although cardiomyocytes release EVs under physiological conditions, cellular stresses caused by hypoxia/reoxygenation or reactive oxygen species enhance EV release and modify the protein profile of EVs [4].

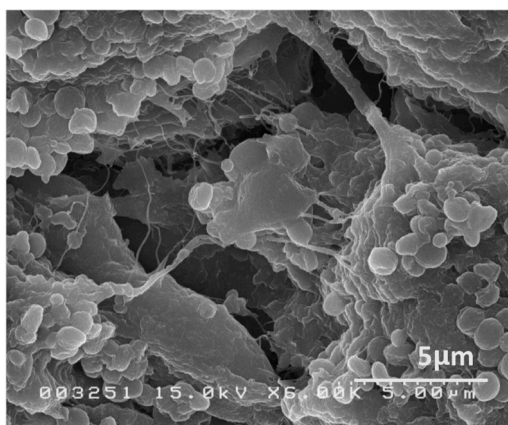


Figure 1. Scanning electron microscopy images of extracellular vesicles (EVs) released from cardiomyocytes. Cardiac tissues from a healthy mouse were collected and prepared (primary fixation with 2.5% glutaraldehyde, secondary fixation with osmium tetroxide, dehydration, mounting, and ion sputter coating). The sample was observed by scanning electron microscope (Hitachi S-4500). [Unpublished data].

2.2. The Structural Properties of EVs

The lipid or protein components of EV membranes determine their biodistribution and uptake by recipient cells [20]. EVs have the lipid bilayer membrane consisting of proteins and lipids with abundant lipid rafts, which are important structures in labeling them with imaging probes. In spite of the similarity to the plasma membrane, EV membranes contain some specific surface lipid components designated for ligand-receptor pairing and resultant cellular uptake of EVs [21]. EVs are enriched with anionic phospholipid phosphatidylserine (PS), which is recognized by macrophages [22–24]. The integrin composition of the membrane renders the affinity with certain tissues [25]. EV surface protein glycosylation affects biodistribution of EVs [26]. EV internalization is caused by several mechanisms such as lipid raft-, clathrin-, and caveolae-dependent endocytosis, micropinocytosis, and phagocytosis [20,27]. The routes of EV uptake could also be affected by EV type or conditions of the extracellular space (acidic/basic, hypoxic, extracellular matrix components). It is likely cells and EVs have some systems that can let EVs escape from the degrading pathways after being taken up by cells [28]. Unmodified EVs suffer from rapid clearance and low accumulation in target tissues and cells. Similar to liposomes, intravenously administered EVs are delivered to the reticuloendothelial system mainly the liver and spleen and are rapidly cleared from circulation via, in part, the macrophage-dependent pathway [29,30].

Exosomes contain common biomarkers such as Alix, tumor susceptibility gene 101 (Tsg101), Annexin XI, and tetraspanins (CD9, CD81, and CD63) [31]. Several proteins such as actinin-4 and mitofilin are more favorably expressed in large or medium-sized EVs [32]. Exosomes and microvesicles share some surface biomarker proteins, including MHC, flotillin, heat-shock proteins, and tetraspanins CD63 and CD9 [32]. On the other hand, vesicular proteins vary from one cell type to the other [33]. The cellular origin of EVs influence surface protein profile including integrin subunits, tetraspanins, and fibronectin [20]. Proteomic analysis revealed that the EVs secreted from adult cardiomyocytes uniquely include cytosolic, sarcomeric, and mitochondrial proteins, such as myomesin, myosin-binding protein C, VCP, tropomyosin, and α -crystallin [34]. The unique protein profiles define different targeting characteristics of EVs.

3. Labeling and Imaging of EVs

3.1. Imaging Modalities of EV Labeling and Tracking

While no ideal imaging technology has been developed for in vivo EV labeling and tracking, rigorous research for EV imaging has been performed utilizing optical imaging (fluorescence

imaging (FLI) and bioluminescence imaging (BLI)), single-photon emission computed tomography (SPECT)/positron emission tomography (PET), and magnetic resonance imaging (MRI). Many kinds of probes or vectors for labeling EVs are available on the market. Each method has its strength and weakness related to the spatial or temporal resolution, sensitivity, specificity, clinical availability, safety, and complexity of the technique. In EV labeling, it is fundamental not to disturb the integrity of the EV membranes in order to maintain their morphology and physiological functions.

The methods for labeling are largely categorized into direct labeling and indirect labeling. In the direct labeling, probes are directly bound to the target (EV) surface or transported inside the cells or EVs via physiological mechanisms. After cells are directly labeled, labeled EVs are created inside the cells and released. One of the advantages of the direct labeling method is that it is simple and relatively physiological without need for any gene modification. In general, the critical problem with direct labeling is that signals may persist longer than the actual lifetime of EVs in the body because of the aggregation or re-binding of the probes by other cells or substrates. By contrast, in indirect labeling, reporter genes such as luciferase or fluorescence binding proteins are transfected with donor cells, followed by the expression of the reporter genes or fluorescence tagged EV membrane proteins. The indirect labeling method could evaluate the in vivo lifetime of EVs and transfer of EV components to the recipient cells more accurately and be suitable for real-time monitoring [35].

3.2. FLI, BLI, and PET/SPECT

FLI has been widely used for labeling EVs. Fluorescent proteins or organic dyes emit signals under excitation with an external light source, which are detected by an in vivo imaging system. Small lipophilic fluorophores are used to label isolated EVs due to its affinity to lipids on the membrane and produce a strong and stable fluorescence signal. PKH67 (Ex. 490 nm/Em. 502 nm), PKH26 (Ex.551 nm/Em. 565 nm), and DiOC₁₈ (7) (DiR) (Ex.750 nm/Em.780 nm) are representative lipophilic carbocyanine dyes used for EV labeling [36–38]. DiR is a Near-infrared (NIR) dye, which is advantageous for in vivo applications due to the high signal to noise ratio (SNR), minimal autofluorescence, and enhanced tissue penetration [39]. However, several drawbacks of the lipophilic dyes are known that make them unideal probes for EV labeling and in vivo tracking. Binding of lipophilic dye is not EV membrane specific. Due to their relatively long in vivo half-life of 5 to >100 days, after degradation of EVs, the dyes remain intact and bind to other lipid components non-specifically in the extracellular space or the recipient cells [40]. The dyes could also promote EV aggregation [41]. As a result, in vivo signal from these lipid dyes yield inaccurate information regarding the fates of EVs compared to signals obtained by BLI [35].

The membrane-targeted indirect labeling methods are also used for FLI. Fluorescent proteins such as green fluorescent protein (GFP) or red fluorescent protein (RFP) fused with membrane protein markers are transfected to donor cells. Cells transfected with CD63-GFP plasmid express GFP-tagged EV membrane anchoring protein [42]. Lai et al. reported a method to fuse fluorescent proteins with a palmitoylation signal of EV membrane [43]. By fusing fluorescent proteins (enhanced GFP or tandem dimer Tomato) with a consensus palmitoylation sequence, these reporters are expressed on the whole cell membrane. This is followed by labeling of EVs of variable sizes on their membranes. Notably, the fused protein was expressed mostly on the inner membrane of EVs, which could avoid potential disturbance to EV surface function. Using this EV labeling technique, they visualized bidirectional cell-cell translocation of EVs. In addition, the implantation of the labeled thymoma cells enabled visualization of EV release from the tumors in vivo, revealing that the tumor releases more EVs in the peripheral regions, accompanying infiltration of immune cells compared to the tumor core area of the highest tumor cell density [43].

BLI is a powerful in vivo optical imaging tool. In BLI, luciferases, most commonly *Photinus pyralis* luciferase (firefly; Fluc), *Renilla reniformis* luciferase (sea pansy; Tluc), and *Gaussia princeps* luciferase (marine copepod; Gluc) are used as reporters. Luciferases emit bioluminescence via oxidation of their respective substrate with either ATP and Mg (Fluc-D-luciferin), or oxygen alone (Rluc and

Gluc-coelenterazine), when the enzyme is expressed in vivo as a molecular reporter [44]. Gluc emit over 1000-fold stronger bioluminescence compared to RLuc and Fluc [45]. Reporter luciferase genes need to be inserted into the genome of the donor cells. BLI has high SNR since the mammalian tissues have little intrinsic bioluminescence. Lai et al. developed a method that transfects donor cells with lentivirus vectors encoding Gluc combined with transmembrane domain [35,46]. EVs that share lipid bilayer components with a cellular membrane then express transmembrane domain bound Gluc. This method has an excellent temporal resolution and enables tracking of the accurate fate of EVs in vivo. Decreased Gluc signal indicates decreased availability of external EVs and internal degradation of Gluc transcripts. EVs accumulated in the kidneys, liver, lungs, and spleen. Intravenously administered EVs have a half-life of < 30 min in most tissues and are cleared from the body by 6 h post injection [35].

The application of BLI and FLI is limited to the small animals because of the limited signal penetration (only several centimeters) [44]. It could give valuable information in preclinical research. The obtained signals are semi-quantitative as signal strength strongly depends on the tissue depth and has limited sensitivity to signals from deep tissues. Another limitation is that the expression level of reporter proteins restricts the fluorescence or bioluminescence signals.

PET/SPECT label substrates with high-energy gamma-emitting radiotracers. They are widely used as clinical imaging tools. PET and SPECT are very sensitive techniques and are extensively used for in vivo tracking of nanomaterials. They rely on detection of high-energy gamma rays, which have no penetration limits. The high energy of emitted photons minimize the attenuation and scattering effects, enabling the accurate quantification of signals in the whole body. PET achieves better sensitivity and spatial resolution compared to SPECT. Although tracers with different half-life and decay profiles are used, short half-life of the radioactive tracers might limit long-term tracking [47]. However, it might not be a problem in EV tracking because of their short lifetime in vivo. Both direct and indirect labeling with ^{99m}Tc or ^{125}I NaI tracers are used to image EVs on SPECT [48,49]. Direct radiolabeling was performed for in vivo real time EV tracking on PET using the commercial ^{124}I NaI probe (half-life >4 days) to form a covalent bond to tyrosine of EV membrane protein [26].

3.3. SPIO and MRI

Compared to the optical imaging or SPECT/PET, MRI has the most exquisite spatial resolution although the sensitivity of MRI is relatively low. MRI without accompanying any radiation exposure is superior to nuclear labeling in terms of safety. The labeling methods developed for MRI can be compatible with clinical application. It can be also combined with simultaneous anatomical assessment, functional evaluation and tissue characterization. This capability enables precise localization of EVs and assessment of their specific regional effects in the different areas of tissue injury to correlate EV engraftment with therapeutic efficacy. The strength and weakness of EV labeling using MRI are summarized in Table 1.

Table 1. Pros and cons of superparamagnetic iron oxide (SPIO) labeling.

Pros	Cons
Clinical translation is easy	False positive signals
Excellent spatial resolution	Low sensitivity
No gene modification required	Real time observation is difficult
No interference with surface membrane	Quantification might not be accurate
No radiation	Whole body scan is not easy
Simultaneous assessment of anatomy/function/ tissue characteristics is possible	Potential interference with cellular/vesicular function

Superparamagnetic iron oxide nanoparticles (SPIO) are magnetic nanoparticles most commonly used for visualizing cells on MRI. It could be applied for EVs in a similar manner. SPIO nanoparticles are attractive probes for EV labeling because of their small size and biocompatibility. SPIO enable detection of labeled objects in the tissues longitudinally. The superparamagnetic core of SPIO produces local field homogeneity, which enhances transverse relaxation ($=T_2^*$ relaxation effect) and produces negative contrast [50]. Large susceptibility effects of SPIO make the signal void much larger than the

particle size, enhancing detectability. Negative contrast in the tissues containing SPIO can be detected on a T2*-weighted gradient echo sequence consisting of long TR/TE and low flip angle [51]. In general, quantification of SPIO accumulation from signal loss on MRI is difficult [52]. T2* mapping can be useful for quantifying accumulation of SPIO, which is created by several gradient echo sequences at different TEs to calculate T2* decrease on the T2* decay curve [14].

SPIO consists of the functional core, coating, and surface properties. Those properties determine the efficiency of cellular uptake, distribution, metabolism, and potential toxicity. The functional core producing the superparamagnetic property is a single-domain iron oxide molecule (<10 nm diameter in general) containing Fe₃O₄ (magnetite), gamma-Fe₂O₃ (maghemite), or alpha-Fe₂O₃ (hematite) [53]. SPIO are coated with biocompatible polymers such as dextran and carboxydextran, which can prevent aggregations, structural changes and degradation [54,55]. SPIO are classified into standard SPIO (SSPIO, >50 nm), ultra-small SPIO (USPIO, 10–50 nm), and very-small SPIO (VSPIO, <10 nm) based on their hydrodynamic diameters [56]. The larger magnetic susceptibility of SSPIO yields larger R2 relaxation and higher T2-shortening effects compared to the effects caused by USPIO [57]. However, the size of USPIO is more suitable for labeling nano-scale EVs (Figure 2). SPIO are clinically used as MRI contrast agents for evaluating blood volume fraction, perfusion, and cancer metastasis [10–12]. Unfortunately, manufacturers of most of them were discontinued because of the safety reasons or infrequent use (Table 2). Currently, ferumoxytol is the only clinically available USPIO. Ferumoxytol is approved by FDA for iron replacement therapy for renal anemia patients. However, it has been also used off-label as an MRI contrast agent [58]. Clinical compatibility of labeling agents is critical in applying EV labeling in humans. Therefore, labeling with ferumoxytol is an attractive method and several groups have reported the method to label cells with ferumoxytol [59,60].

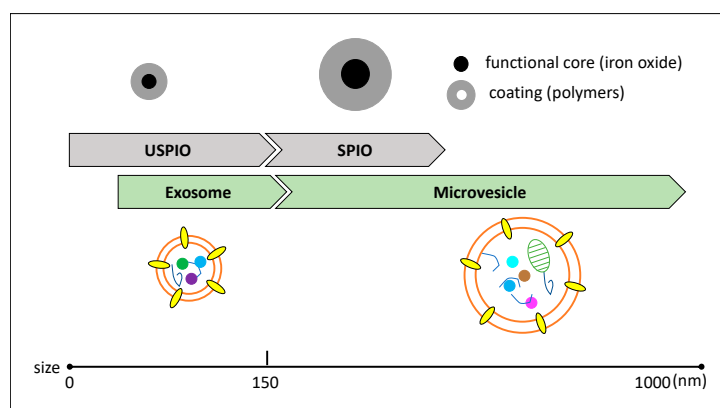


Figure 2. Comparison of size between ultra-small SPIO (USPIO) and SPIO (upper), and exosome and microvesicles (lower). [Unpublished figure].

Table 2. Clinical SPIO (cited from [61]).

Generic Name	Brand Name	Classification	Coating	Diameter (nm)	Status
Ferumoxide	Feridex/Endorem	SSPIO	dextran	120-180	discontinued
Ferumoxtran-10	Combidx/Sinerem	USPIO	dextran	15-30	discontinued
Ferucarbotran	Resovist/Cliavist	SSPIO	carboxydextran	60	discontinued
Ferucarbotran	Supravist	USPIO	carboxydextran	21	discontinued
Feruglose	Clariscan	USPIO	pegylated starch	20	discontinued
Ferumoxytol	Feraheme	USPIO	carboxymethyl dextran	30	FDA approved

3.4. EV Labeling with SPIO

SPIO can label cells directly. Subsequently, labeled EVs are created inside the cells and released. In this method, donor cells are incubated with the culture medium containing SPIO. Most of the cell types except for phagocytes such as neutrophils and macrophages do not have the capacity of

phagocytizing particles. Therefore, iron-oxide nanoparticles are prepared with facilitators such as poly-L-Lysine, protamine, or some transfection reagents, which facilitate cellular uptake of SPIO [62]. These cationic compounds facilitate interaction of SPIO with the negatively charged cell membrane and subsequent endosomal uptake mainly by Clathrin-mediated endocytosis [27]. Most cell types without phagocytizing capacity can be labeled by this method. Donor cells which incorporate SPIO then release vesicles containing SPIO. USPIO taken up by human bone marrow derived MSC (hBM-MSCs) were found to traffic to the intracellular vesicles expressing EV markers such as CD9, CD63, and CD81, which indicated that the intracellular localization of internalized SPIOs is actively regulated and the deposited SPIO are ready to be released from cells [63]. The SPIO internalization can be confirmed by electron microscopy (Figure 3). Accumulation of SPIO labeled EVs in the tissue is detected on T2*-weighted MRI (Figure 3). Busato et al. labeled exosomes isolated from adipose stem cells with commercial USPIO by this cell labeling method. They injected isolated labeled exosomes in the hindlimb and detected them on MRI [64,65]. They labeled cells with 200 $\mu\text{gFe/mL}$ of USPIO and found 0.634 μg of iron was contained per 100 μg of exosomes. Injection of 5 μg of exosomes produced sufficient signals to detect on MRI. Histologically, Prussian Blue staining confirms the existence of SPIO in the tissue (Figure 3). The amount of SPIO internalization depends on the incubation time (cell and SPIO) and the iron concentration [64]. EV iron content is significantly correlated with intracellular iron content. Therefore, a strategy should be made to label donor cells with the highest SPIO concentration possible [65]. T2* negative contrast depends on the concentration of loaded SPIO in the vesicles and the number of labeled exosomes.

The labeled EVs had the similar capacity of being taken up by cells in vitro [63]. This direct SPIO labeling method is likely to maintain the morphology and the physiological characteristics of the EVs intact. The major limitation of SPIO-labeling is the persistence of in vivo signal after EV degradation. Signals from EVs labeled with SPIO cannot be distinguished from signals originating from other cells taking up SPIO after EV degradation. In the past report, significant MRI signal was derived from SPIO-containing macrophages 3 weeks after transplantation of SPIO-labeled cells despite only a few viable transplanted cells remaining in the tissue [66].

Another representative method to label EV with SPIO is the direct vesicle labeling via electroporation. Hu et al. labeled melanoma exosomes with USPIO (SPION5, 4.5 nm in diameter) by electroporation. Labeled melanoma exosomes were injected into the foot pad and their migration into the ipsilateral local lymph node was detected 48 h post injection by T2* mapping [67]. The potential disadvantage of electroporation method is that this could damage the membrane as the strong electric field by electroporation causes pore formation in the EV membrane to let iron oxide particles be inside [68].

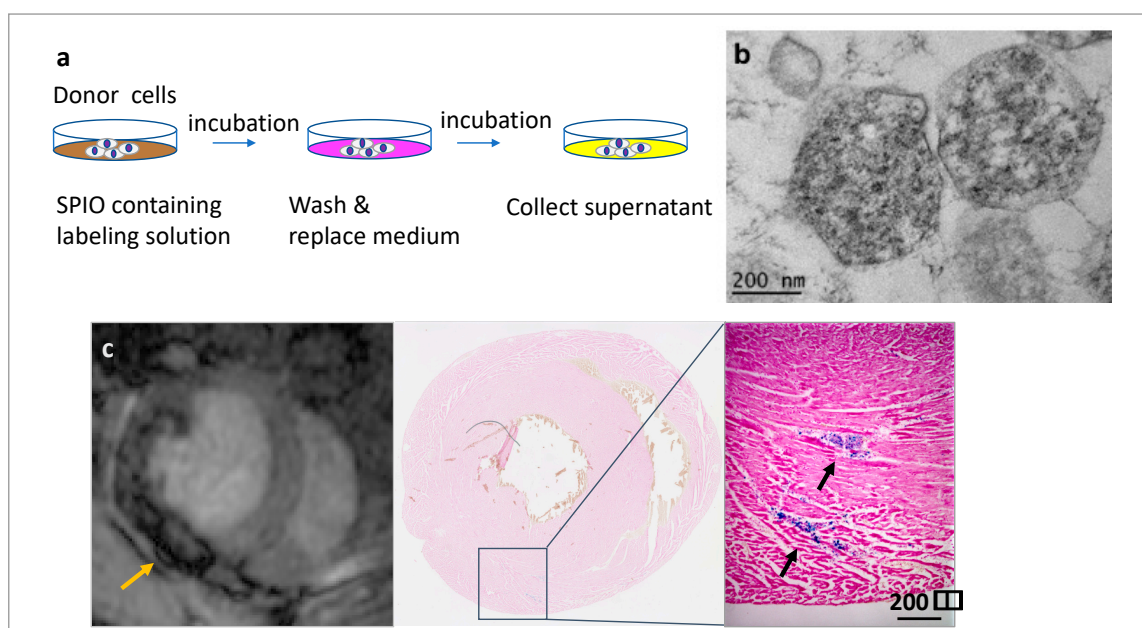


Figure 3. (a) The diagram of the method of labeling with SPIO. (b) Transmission electron microscopy of labeled extracellular vesicles (EVs). SPIO are detected as black particles inside the vesicles. (c) In vivo magnetic resonance imaging (MRI) detection of SPIO labeled EVs injected in the mouse heart (left). The image was acquired with a GE 3.0T Signa scanner. Prussian blue staining of the slice from the excised heart (middle) proved the iron oxide particles stained blue in the myocardium (right: high magnification). [Unpublished data].

3.5. Effects of Labeling on the Functions of EVs

SPIO generally has low toxicity to cells. However, some in vitro experiments suggested the possibility that iron oxide or the facilitators could cause cellular stress (mitochondrial dysfunction and reactive oxygen species generation), alterations in gene expression and cell differentiation, decreased cell proliferation, and promotion of pro-inflammatory environment, depending on their concentrations [69]. Cellular/vesicular iron concentration could interfere with cell viability and production of EVs. Therefore, the optimization of iron concentration, incubation time, cell viability, and MRI image contrast are the crucial points [65]. Further research will be required to clarify the effect of SPIO on EVs.

4. Summary and Outlook

Technology to image EVs are developing rapidly and more and more labeling probes are becoming available. They are useful for visualizing intercellular EV translocations and biodistribution of implanted EVs in preclinical small animal models. It is important to select the appropriate labeling method and imaging modality based on the purpose. Labeling of EVs with SPIO for MRI detection is clinically compatible and especially useful when specific organs are targeted. It has limitations in real-time monitoring and whole-body imaging. EV labeling using SPIO has just started and further studies are needed in the future to establish the method and its usefulness. The SPIO signal on MRI needs to be verified by precise histological evaluation and comparison with signals obtained from in vivo real-time monitoring using BLI, FLI, or SPECT/PET.

Advancement of the EV imaging technology could strongly help understand the functions and kinetics of EVs, and which in turn, help advance imaging techniques. Further studies are necessary, focusing on labeling of various kinds of EVs with different origins and targets, gaining more stable and stronger signals, utilizing completely biocompatible methods with high safety, improving the detection and quantification method, and enabling accurate real-time monitoring.

EV labeling and tracking will give us valuable information when we try to apply them as drug delivery systems. However, current technologies rely on the labeling of the external EVs and it is quite challenging to visualize the biodistributions of internal EVs. A more comprehensive approach is required to truly understand the roles of EVs.

Author Contributions: Y.T.; writing—original draft preparation, P.C.Y.; writing—review and editing.

Funding: NIH UM1 (P.Y.); NIH K24 (P.Y.).

Conflicts of Interest: The authors declare no conflict of interest.

References

1. Kourembanas, S. Exosomes: Vehicles of intercellular signaling, biomarkers, and vectors of cell therapy. *Annu. Rev. Physiol.* **2015**, *77*, 13–27. [[CrossRef](#)]
2. Torralba, D.; Baixauli, F.; Sánchez-Madrid, F. Mitochondria Know No Boundaries: Mechanisms and Functions of Intercellular Mitochondrial Transfer. *Front. Cell Dev. Biol.* **2016**, *4*, 107. [[CrossRef](#)]
3. Coly, P.M.; Boulanger, C.M. Extracellular Mitochondria and Vesicles. *Circ. Res.* **2019**, *125*, 53–54. [[CrossRef](#)] [[PubMed](#)]
4. Cervio, E.; Barile, L.; Moccetti, T.; Vassalli, G. Exosomes for Intramyocardial Intercellular Communication. *Stem Cells Int.* **2015**, *2015*, 482171. [[CrossRef](#)] [[PubMed](#)]
5. Bang, C.; Batkai, S.; Dangwal, S.; Gupta, S.K.; Foinquinos, A.; Holzmann, A.; Just, A.; Remke, J.; Zimmer, K.; Zeug, A.; et al. Cardiac fibroblast-derived microRNA passenger strand-enriched exosomes mediate cardiomyocyte hypertrophy. *J. Clin. Investig.* **2014**, *124*, 2136–2146. [[CrossRef](#)] [[PubMed](#)]
6. Halkein, J.; Tabruyn, S.P.; Ricke-Hoch, M.; Haghikia, A.; Nguyen, N.Q.; Scherr, M.; Castermans, K.; Malvaux, L.; Lambert, V.; Thiry, M.; et al. MicroRNA-146a is a therapeutic target and biomarker for peripartum cardiomyopathy. *J. Clin. Investig.* **2013**, *123*, 2143–2154. [[CrossRef](#)] [[PubMed](#)]
7. Sahoo, S.; Klychko, E.; Thorne, T.; Misener, S.; Schultz, K.M.; Millay, M.; Ito, A.; Liu, T.; Kamide, C.; Agrawal, H.; et al. Exosomes from human CD34(+) stem cells mediate their proangiogenic paracrine activity. *Circ. Res.* **2011**, *109*, 724–728. [[CrossRef](#)] [[PubMed](#)]
8. Timmers, L.; Lim, S.K.; Arslan, F.; Armstrong, J.S.; Hoefler, I.E.; Doevendans, P.A.; Piek, J.J.; El Oakley, R.M.; Choo, A.; Lee, C.N.; et al. Reduction of myocardial infarct size by human mesenchymal stem cell conditioned medium. *Stem Cell Res.* **2007**, *1*, 129–137. [[CrossRef](#)] [[PubMed](#)]
9. Arslan, F.; Lai, R.C.; Smeets, M.B.; Akeroyd, L.; Choo, A.; Aguor, E.N.; Timmers, L.; van Rijen, H.V.; Doevendans, P.A.; Pasterkamp, G.; et al. Mesenchymal stem cell-derived exosomes increase ATP levels, decrease oxidative stress and activate PI3K/Akt pathway to enhance myocardial viability and prevent adverse remodeling after myocardial ischemia/reperfusion injury. *Stem Cell Res.* **2013**, *10*, 301–312. [[CrossRef](#)]
10. Finn, J.P.; Nguyen, K.L.; Han, F.; Zhou, Z.; Salusky, I.; Ayad, I.; Hu, P. Cardiovascular MRI with ferumoxytol. *Clin. Radiol.* **2016**, *71*, 796–806. [[CrossRef](#)]
11. Rivera-Rivera, L.A.; Schubert, T.; Johnson, K.M. Measurements of cerebral blood volume using quantitative susceptibility mapping, R. *NMR Biomed.* **2019**, e4175. [[CrossRef](#)] [[PubMed](#)]
12. Toth, G.B.; Varallyay, C.G.; Horvath, A.; Bashir, M.R.; Choyke, P.L.; Daldrup-Link, H.E.; Dosa, E.; Finn, J.P.; Gahramanov, S.; Harisinghani, M.; et al. Current and potential imaging applications of ferumoxytol for magnetic resonance imaging. *Kidney Int.* **2017**, *92*, 47–66. [[CrossRef](#)] [[PubMed](#)]
13. Huang, Z.; Li, C.; Yang, S.; Xu, J.; Shen, Y.; Xie, X.; Dai, Y.; Lu, H.; Gong, H.; Sun, A.; et al. Magnetic resonance hypointensive signal primarily originates from extracellular iron particles in the long-term tracking of mesenchymal stem cells transplanted in the infarcted myocardium. *Int. J. Nanomed.* **2015**, *10*, 1679–1690. [[CrossRef](#)]
14. Bos, C.; Delmas, Y.; Desmoulière, A.; Solanilla, A.; Hauger, O.; Grosset, C.; Dubus, I.; Ivanovic, Z.; Rosenbaum, J.; Charbord, P.; et al. In vivo MR imaging of intravascularly injected magnetically labeled mesenchymal stem cells in rat kidney and liver. *Radiology* **2004**, *233*, 781–789. [[CrossRef](#)]
15. Mathiasen, A.B.; Hansen, L.; Friis, T.; Thomsen, C.; Bhakoo, K.; Kastrup, J. Optimal labeling dose, labeling time, and magnetic resonance imaging detection limits of ultrasmall superparamagnetic iron-oxide nanoparticle labeled mesenchymal stromal cells. *Stem Cells Int.* **2013**, *2013*, 353105. [[CrossRef](#)]

16. Zaborowski, M.P.; Balaj, L.; Breakefield, X.O.; Lai, C.P. Extracellular Vesicles: Composition, Biological Relevance, and Methods of Study. *Bioscience* **2015**, *65*, 783–797. [[CrossRef](#)]
17. Van Niel, G.; D'Angelo, G.; Raposo, G. Shedding light on the cell biology of extracellular vesicles. *Nat. Rev. Mol. Cell Biol.* **2018**, *19*, 213–228. [[CrossRef](#)]
18. Colombo, M.; Raposo, G.; Théry, C. Biogenesis, secretion, and intercellular interactions of exosomes and other extracellular vesicles. *Annu. Rev. Cell Dev. Biol.* **2014**, *30*, 255–289. [[CrossRef](#)]
19. Gupta, S.; Knowlton, A.A. HSP60 trafficking in adult cardiac myocytes: Role of the exosomal pathway. *Am. J. Physiol. Heart Circ. Physiol.* **2007**, *292*, H3052–H3056. [[CrossRef](#)]
20. Murphy, D.E.; de Jong, O.G.; Brouwer, M.; Wood, M.J.; Lavieu, G.; Schiffelers, R.M.; Vader, P. Extracellular vesicle-based therapeutics: Natural versus engineered targeting and trafficking. *Exp. Mol. Med.* **2019**, *51*, 32. [[CrossRef](#)]
21. Théry, C.; Ostrowski, M.; Segura, E. Membrane vesicles as conveyors of immune responses. *Nat. Rev. Immunol.* **2009**, *9*, 581–593. [[CrossRef](#)] [[PubMed](#)]
22. Matsumoto, A.; Takahashi, Y.; Nishikawa, M.; Sano, K.; Morishita, M.; Charoenviriyakul, C.; Saji, H.; Takakura, Y. Role of Phosphatidylserine-Derived Negative Surface Charges in the Recognition and Uptake of Intravenously Injected B16BL6-Derived Exosomes by Macrophages. *J. Pharm. Sci.* **2017**, *106*, 168–175. [[CrossRef](#)] [[PubMed](#)]
23. Zwaal, R.F.; Bevers, E.M.; Comfurius, P.; Rosing, J.; Tilly, R.H.; Verhallen, P.F. Loss of membrane phospholipid asymmetry during activation of blood platelets and sickled red cells; mechanisms and physiological significance. *Mol. Cell Biochem.* **1989**, *91*, 23–31. [[CrossRef](#)] [[PubMed](#)]
24. Miyanishi, M.; Tada, K.; Koike, M.; Uchiyama, Y.; Kitamura, T.; Nagata, S. Identification of Tim4 as a phosphatidylserine receptor. *Nature* **2007**, *450*, 435–439. [[CrossRef](#)] [[PubMed](#)]
25. Hoshino, A.; Costa-Silva, B.; Shen, T.L.; Rodrigues, G.; Hashimoto, A.; Tesic Mark, M.; Molina, H.; Kohsaka, S.; Di Giannatale, A.; Ceder, S.; et al. Tumour exosome integrins determine organotropic metastasis. *Nature* **2015**, *527*, 329–335. [[CrossRef](#)]
26. Royo, F.; Cossío, U.; Ruiz de Angulo, A.; Llop, J.; Falcon-Perez, J.M. Modification of the glycosylation of extracellular vesicles alters their biodistribution in mice. *Nanoscale* **2019**, *11*, 1531–1537. [[CrossRef](#)]
27. Hillaireau, H.; Couvreur, P. Nanocarriers' entry into the cell: Relevance to drug delivery. *Cell Mol. Life Sci.* **2009**, *66*, 2873–2896. [[CrossRef](#)]
28. Izquierdo-Useros, N.; Naranjo-Gómez, M.; Archer, J.; Hatch, S.C.; Erkizia, I.; Blanco, J.; Borràs, F.E.; Puertas, M.C.; Connor, J.H.; Fernández-Figueras, M.T.; et al. Capture and transfer of HIV-1 particles by mature dendritic cells converges with the exosome-dissemination pathway. *Blood* **2009**, *113*, 2732–2741. [[CrossRef](#)]
29. Charoenviriyakul, C.; Takahashi, Y.; Morishita, M.; Matsumoto, A.; Nishikawa, M.; Takakura, Y. Cell type-specific and common characteristics of exosomes derived from mouse cell lines: Yield, physicochemical properties, and pharmacokinetics. *Eur. J. Pharm. Sci.* **2017**, *96*, 316–322. [[CrossRef](#)]
30. Abra, R.M.; Hunt, C.A. Liposome disposition in vivo. III. Dose and vesicle-size effects. *Biochim. Biophys. Acta* **1981**, *666*, 493–503. [[CrossRef](#)]
31. Lötvall, J.; Hill, A.F.; Hochberg, F.; Buzás, E.I.; Di Vizio, D.; Gardiner, C.; Gho, Y.S.; Kurochkin, I.V.; Mathivanan, S.; Quesenberry, P.; et al. Minimal experimental requirements for definition of extracellular vesicles and their functions: A position statement from the International Society for Extracellular Vesicles. *J. Extracell. Vesicles* **2014**, *3*, 26913. [[CrossRef](#)] [[PubMed](#)]
32. Kowal, J.; Arras, G.; Colombo, M.; Jouve, M.; Morath, J.P.; Primdal-Bengtson, B.; Dingli, F.; Loew, D.; Tkach, M.; Théry, C. Proteomic comparison defines novel markers to characterize heterogeneous populations of extracellular vesicle subtypes. *Proc. Natl. Acad. Sci. USA* **2016**, *113*, E968–E977. [[CrossRef](#)] [[PubMed](#)]
33. Dickhout, A.; Koenen, R.R. Extracellular Vesicles as Biomarkers in Cardiovascular Disease; Chances and Risks. *Front. Cardiovasc. Med.* **2018**, *5*, 113. [[CrossRef](#)] [[PubMed](#)]
34. Malik, Z.A.; Kott, K.S.; Poe, A.J.; Kuo, T.; Chen, L.; Ferrara, K.W.; Knowlton, A.A. Cardiac myocyte exosomes: Stability, HSP60, and proteomics. *Am. J. Physiol. Heart Circ. Physiol.* **2013**, *304*, H954–H965. [[CrossRef](#)] [[PubMed](#)]
35. Lai, C.P.; Mardini, O.; Ericsson, M.; Prabhakar, S.; Maguire, C.; Chen, J.W.; Tannous, B.A.; Breakefield, X.O. Dynamic biodistribution of extracellular vesicles in vivo using a multimodal imaging reporter. *ACS Nano* **2014**, *8*, 483–494. [[CrossRef](#)]

36. Liu, H.; Gao, W.; Yuan, J.; Wu, C.; Yao, K.; Zhang, L.; Ma, L.; Zhu, J.; Zou, Y.; Ge, J. Exosomes derived from dendritic cells improve cardiac function via activation of CD4 (+) T lymphocytes after myocardial infarction. *J. Mol. Cell Cardiol.* **2016**, *91*, 123–133. [[CrossRef](#)]
37. Usman, W.M.; Pham, T.C.; Kwok, Y.Y.; Vu, L.T.; Ma, V.; Peng, B.; Chan, Y.S.; Wei, L.; Chin, S.M.; Azad, A.; et al. Efficient RNA drug delivery using red blood cell extracellular vesicles. *Nat. Commun.* **2018**, *9*, 2359. [[CrossRef](#)]
38. Wiklander, O.P.; Nordin, J.Z.; O’Loughlin, A.; Gustafsson, Y.; Corso, G.; Mäger, I.; Vader, P.; Lee, Y.; Sork, H.; Seow, Y.; et al. Extracellular vesicle in vivo biodistribution is determined by cell source, route of administration and targeting. *J. Extracell. Vesicles* **2015**, *4*, 26316. [[CrossRef](#)]
39. Di Rocco, G.; Baldari, S.; Toietta, G. Towards Therapeutic Delivery of Extracellular Vesicles: Strategies for. *Stem Cells Int.* **2016**, *2016*, 5029619. [[CrossRef](#)]
40. Rieck, B. Unexpected durability of PKH 26 staining on rat adipocytes. *Cell Biol. Int.* **2003**, *27*, 445–447. [[CrossRef](#)]
41. Pužar Dominkuš, P.; Stenovec, M.; Sitar, S.; Lasič, E.; Zorec, R.; Plemenitaš, A.; Žagar, E.; Kreft, M.; Lenassi, M. PKH26 labeling of extracellular vesicles: Characterization and cellular internalization of contaminating PKH26 nanoparticles. *Biochim. Biophys. Acta Biomembr.* **2018**, *1860*, 1350–1361. [[CrossRef](#)]
42. Suetsugu, A.; Honma, K.; Saji, S.; Moriwaki, H.; Ochiya, T.; Hoffman, R.M. Imaging exosome transfer from breast cancer cells to stroma at metastatic sites in orthotopic nude-mouse models. *Adv. Drug Deliv. Rev.* **2013**, *65*, 383–390. [[CrossRef](#)]
43. Lai, C.P.; Kim, E.Y.; Badr, C.E.; Weissleder, R.; Mempel, T.R.; Tannous, B.A.; Breakefield, X.O. Visualization and tracking of tumour extracellular vesicle delivery and RNA translation using multiplexed reporters. *Nat. Commun.* **2015**, *6*, 7029. [[CrossRef](#)]
44. Sadikot, R.T.; Blackwell, T.S. Bioluminescence imaging. *Proc. Am. Thorac. Soc.* **2005**, *2*, 537–540. [[CrossRef](#)]
45. Badr, C.E.; Tannous, B.A. Bioluminescence imaging: Progress and applications. *Trends Biotechnol.* **2011**, *29*, 624–633. [[CrossRef](#)]
46. Lai, C.P.; Tannous, B.A.; Breakefield, X.O. Noninvasive in vivo monitoring of extracellular vesicles. *Methods Mol. Biol.* **2014**, *1098*, 249–258. [[CrossRef](#)]
47. Velly, H.; Bouix, M.; Passot, S.; Penicaud, C.; Beinsteiner, H.; Ghorbal, S.; Lieben, P.; Fonseca, F. Cyclopropanation of unsaturated fatty acids and membrane rigidification improve the freeze-drying resistance of *Lactococcus lactis* subsp. *lactis* TOMSC161. *Appl. Microbiol. Biotechnol.* **2015**, *99*, 907–918. [[CrossRef](#)]
48. Varga, Z.; Gyurkó, I.; Pálóczi, K.; Buzás, E.I.; Horváth, I.; Hegedűs, N.; Máthé, D.; Szigeti, K. Radiolabeling of Extracellular Vesicles with (99m)Tc for Quantitative In Vivo Imaging Studies. *Cancer Biother. Radiopharm.* **2016**, *31*, 168–173. [[CrossRef](#)]
49. Morishita, M.; Takahashi, Y.; Nishikawa, M.; Sano, K.; Kato, K.; Yamashita, T.; Imai, T.; Saji, H.; Takakura, Y. Quantitative analysis of tissue distribution of the B16BL6-derived exosomes using a streptavidin-lactadherin fusion protein and iodine-125-labeled biotin derivative after intravenous injection in mice. *J. Pharm. Sci.* **2015**, *104*, 705–713. [[CrossRef](#)]
50. Ghugre, N.R.; Coates, T.D.; Nelson, M.D.; Wood, J.C. Mechanisms of tissue-iron relaxivity: Nuclear magnetic resonance studies of human liver biopsy specimens. *Magn. Reson. Med.* **2005**, *54*, 1185–1193. [[CrossRef](#)]
51. Nitz, W.R.; Reimer, P. Contrast mechanisms in MR imaging. *Eur. Radiol.* **1999**, *9*, 1032–1046. [[CrossRef](#)] [[PubMed](#)]
52. Li, Z.; Suzuki, Y.; Huang, M.; Cao, F.; Xie, X.; Connolly, A.J.; Yang, P.C.; Wu, J.C. Comparison of reporter gene and iron particle labeling for tracking fate of human embryonic stem cells and differentiated endothelial cells in living subjects. *Stem Cells* **2008**, *26*, 864–873. [[CrossRef](#)] [[PubMed](#)]
53. Thorek, D.L.; Chen, A.K.; Czupryna, J.; Tsourkas, A. Superparamagnetic iron oxide nanoparticle probes for molecular imaging. *Ann. Biomed. Eng.* **2006**, *34*, 23–38. [[CrossRef](#)]
54. Moraes, L.; Vasconcelos-dos-Santos, A.; Santana, F.C.; Godoy, M.A.; Rosado-de-Castro, P.H.; Jasmin; Azevedo-Pereira, R.L.; Cintra, W.M.; Gasparetto, E.L.; Santiago, M.F.; et al. Neuroprotective effects and magnetic resonance imaging of mesenchymal stem cells labeled with SPION in a rat model of Huntington’s disease. *Stem Cell Res.* **2012**, *9*, 143–155. [[CrossRef](#)]

55. Bull, E.; Madani, S.Y.; Sheth, R.; Seifalian, A.; Green, M.; Seifalian, A.M. Stem cell tracking using iron oxide nanoparticles. *Int. J. Nanomed.* **2014**, *9*, 1641–1653. [[CrossRef](#)]
56. Thorek, D.L.; Tsourkas, A. Size, charge and concentration dependent uptake of iron oxide particles by non-phagocytic cells. *Biomaterials* **2008**, *29*, 3583–3590. [[CrossRef](#)]
57. Metz, S.; Bonaterra, G.; Rudelius, M.; Settles, M.; Rummeny, E.J.; Daldrup-Link, H.E. Capacity of human monocytes to phagocytose approved iron oxide MR contrast agents in vitro. *Eur. Radiol.* **2004**, *14*, 1851–1858. [[CrossRef](#)]
58. Vasanawala, S.S.; Nguyen, K.L.; Hope, M.D.; Bridges, M.D.; Hope, T.A.; Reeder, S.B.; Bashir, M.R. Safety and technique of ferumoxytol administration for MRI. *Magn. Reson. Med.* **2016**, *75*, 2107–2111. [[CrossRef](#)]
59. Thu, M.S.; Bryant, L.H.; Coppola, T.; Jordan, E.K.; Budde, M.D.; Lewis, B.K.; Chaudhry, A.; Ren, J.; Varma, N.R.; Arbab, A.S.; et al. Self-assembling nanocomplexes by combining ferumoxytol, heparin and protamine for cell tracking by magnetic resonance imaging. *Nat. Med.* **2012**, *18*, 463–467. [[CrossRef](#)]
60. Castaneda, R.T.; Khurana, A.; Khan, R.; Daldrup-Link, H.E. Labeling stem cells with ferumoxytol, an FDA-approved iron oxide nanoparticle. *J. Vis. Exp.* **2011**, e3482. [[CrossRef](#)]
61. Jung, J.-H.; Tada, Y.; Yang, P.C. Novel MRI Contrast from Magnetotactic Bacteria to Evaluate In Vivo Stem Cell Engraftment. In *Biological, Physical and Technical Basics of Cell Engineering*; Springer: Singapore, 2018; pp. 365–380.
62. Suzuki, Y.; Zhang, S.; Kundu, P.; Yeung, A.C.; Robbins, R.C.; Yang, P.C. In vitro comparison of the biological effects of three transfection methods for magnetically labeling mouse embryonic stem cells with ferumoxides. *Magn. Reson. Med.* **2007**, *57*, 1173–1179. [[CrossRef](#)]
63. Dabrowska, S.; Del Fattore, A.; Karnas, E.; Frontczak-Baniewicz, M.; Kozłowska, H.; Muraca, M.; Janowski, M.; Lukomska, B. Imaging of extracellular vesicles derived from human bone marrow mesenchymal stem cells using fluorescent and magnetic labels. *Int. J. Nanomed.* **2018**, *13*, 1653–1664. [[CrossRef](#)]
64. Busato, A.; Bonafede, R.; Bontempi, P.; Scambi, I.; Schiaffino, L.; Benati, D.; Malatesta, M.; Sbarbati, A.; Marzola, P.; Mariotti, R. Magnetic resonance imaging of ultrasmall superparamagnetic iron oxide-labeled exosomes from stem cells: A new method to obtain labeled exosomes. *Int. J. Nanomed.* **2016**, *11*, 2481–2490. [[CrossRef](#)]
65. Busato, A.; Bonafede, R.; Bontempi, P.; Scambi, I.; Schiaffino, L.; Benati, D.; Malatesta, M.; Sbarbati, A.; Marzola, P.; Mariotti, R. Labeling and Magnetic Resonance Imaging of Exosomes Isolated from Adipose Stem Cells. *Curr. Protoc. Cell Biol.* **2017**, *75*, 3.44.1–3.44.15. [[CrossRef](#)]
66. Terrovitis, J.; Stuber, M.; Youssef, A.; Preece, S.; Leppo, M.; Kizana, E.; Schär, M.; Gerstenblith, G.; Weiss, R.G.; Marbán, E.; et al. Magnetic resonance imaging overestimates ferumoxide-labeled stem cell survival after transplantation in the heart. *Circulation* **2008**, *117*, 1555–1562. [[CrossRef](#)]
67. Hu, L.; Wickline, S.A.; Hood, J.L. Magnetic resonance imaging of melanoma exosomes in lymph nodes. *Magn. Reson. Med.* **2015**, *74*, 266–271. [[CrossRef](#)]
68. Johnsen, K.B.; Gudbergsson, J.M.; Skov, M.N.; Christiansen, G.; Gurevich, L.; Moos, T.; Duroux, M. Evaluation of electroporation-induced adverse effects on adipose-derived stem cell exosomes. *Cytotechnology* **2016**, *68*, 2125–2138. [[CrossRef](#)]
69. Jasmin; Torres, A.L.; Nunes, H.M.; Passipieri, J.A.; Jelicks, L.A.; Gasparetto, E.L.; Spray, D.C.; Campos de Carvalho, A.C.; Mendez-Otero, R. Optimized labeling of bone marrow mesenchymal cells with superparamagnetic iron oxide nanoparticles and in vivo visualization by magnetic resonance imaging. *J. Nanobiotechnol.* **2011**, *9*, 4. [[CrossRef](#)]

